Author/s:
Ashokan, A;Mulvaney, P

Title:
Spectroelectrochemistry of Colloidal CdSe Quantum Dots

Date:
2021-02-23

Citation:
Ashokan, A. & Mulvaney, P. (2021). Spectroelectrochemistry of Colloidal CdSe Quantum Dots. Chemistry of Materials, 33 (4), pp.1353-1362. https://doi.org/10.1021/acs.chemmater.0c04416.

Persistent Link:
https://hdl.handle.net/11343/344944

Spectroelectrochemistry of Colloidal CdSe Quantum Dots

Arun Ashokan and Paul Mulvaney*

ARC Centre of Excellence in Exciton Science, School of Chemistry, University of Melbourne, Parkville, Victoria 3010, Australia

E-mail: mulvaney@unimelb.edu.au

Abstract

Solution phase spectroelectrochemistry was used to study electron injection into colloidal CdSe quantum dots (QDs) with sizes ranging from 3.4 - 11.1 nm in tetrohydrofuran (THF). The absorbance and photoluminescence of the QDs were monitored in response to both charging and discharging cycles and the optical changes were reversible over a timescale of minutes. Bleaching of the QD $1S_{3/2h}1S_e$ exciton state was used to determine the conduction band energy levels. We found that the negative trion state was stable in THF for hours at a time. Both the degree of bleaching and the recovery of the exciton state depended on the applied potential. Using the Cottrell equation, we found that between ten and one hundred and fifty electrons were injected into the QDs, depending on the electrode potential. Most of the electron injection occurred below the band edge and led to quenching of the QD photoluminescence. The potential at which injection into these trap states occurred depended the QD surface chemistry.

1. Introduction

During photoredox reactions in semiconductor quantum dots (QDs), the nanocrystals exchange electrons and holes with the environment.[1–3] The photogenerated charge carriers are usually unstable and undergo various chemical reactions with oxygen, the solvent or the semiconductor lattice.[4–7] Excess charge carriers directly influence the PL through Auger recombination but also indirectly may generate surface recombination centres.[8,9] These multiple pathways make an understanding of the QD interface complex. In the past, electrons have been injected into QDs in solution using reducing agents or electrically into films of nanocrystals.[10–16] Both of these methods have limitations. In the case of QD films, electron migration between particles is poorly controlled and depends on ligand chemistry and particle packing, while in solution, chemical reducing agents cannot be turned on and off.[10,15] An alternative approach is to undertake direct electrochemistry of the QDs in solution. This has been employed previously to explore the electronic structure of QDs.[17–19] However, electrochemistry of CdE QDs (E = S, Se, Te) has generated mixed results. Some studies found that oxidation and reduction during cyclic voltammetry (CV) was irreversible and this was proposed to originate from a multielectron charge transfer coupled to a fast chemical reaction.[20–22] Conversely, quasi-reversible charge transfer was observed during CV of CdSe QDs dispersed in ionic liquids and complementary redox peaks were also observed with CdTe QDs in organic solvents.[23,24] Reversible electrochemistry has been observed in thin films of mercury chalcogenide QDs.[25] Hence, it is still unclear whether electron transfer between an electrode and a QD in solution is reversible. A related question in this regard is what happens to the charge carrier once injected into the QD. It has been reported that injected charges induce ligand loss from the QD surface and redox reaction of surface atoms.[20,26,27] This may generate new trap states, which in turn alter the optical properties of the QD.[28,29] The primary limitation with direct QD electrochemistry is that the currents are often extremely small. Spectroelectrochemistry (SEC) can be used to obviate some of these problems. This technique has been used to study surface plasmon shifts in metal nanocrystals,[30,31]

electrochromism,[32] blinking,[33] photobrightening[34] and to determine the energy levels of the conduction band of semiconductor nanocrystals.[35,36] In solution phase, this method allows key questions to be answered about the semiconductor and the environment. For example, it is useful to know whether the trion state can be stabilised and whether electrons can be injected and extracted from an electrode reversibly.

In this work, we use solution phase spectroelectrochemistry to measure the optical properties of CdSe QDs in response to electron charging and correlate the observed spectroscopic changes with electrochemical parameters such as potential and current. The honeycomb electrode configuration allows quantification of the charge injection process. The conduction band positions of QDs are deduced from the bleaching of exciton absorption during the filling of conduction band states while the traps states are identified by combining the absorbance bleaching, photoluminescence (PL) quenching and the onset of electron transfer during charging. The optical shifts can be used to determine the stability of the trion state, which is a key state involved in fluorescence blinking.[33]

2. Experimental Methods

Zincblende CdSe nanocrystals were synthesized according to literature procedures with slight modifications.[37] Briefly, 1 mmol of Cd oleate (0.5 M) was dissolved in 5 mL octadecene (ODE) and heated to 120^{o}C. 1 mmol of Se-ODE (0.1M) was injected swiftly into the reaction mixture at 270^{o}C . The reaction was stopped after obtaining the desired size. The crystals were purified by precipitation with ethanol and subsequent resuspension in hexane or toluene. Ligand exchange with trioctylphosphine (TOP) was achieved by adding 2 ml TOP to QDs dispersed in 3 mL toluene and stirring overnight. It was then purified by washing with ethanol.

CdSe/CdS(2ML) and CdSe/ZnS(2ML) synthesis: Core-shell particles were syn-

thesized by using the method described by Kirkwood et al.[38] 25 nmol of CdSe cores (d = 5.24 nm, λ_{abs} = 614 nm) were dispersed in ODE. The corresponding metal oleate and octanethiol were added using a syringe pump at 300^{o}C. After the reaction, the core-shell QDs were precipitated by the addition of an acetone-ethanol mixture. The particles were then redispersed in hexane for further experiments.

Characterization: Steady state absorption spectra and the fluorescence spectra were collected with an Agilent HP8453 UV-Vis Spectrometer and a Fluorolog Spectrofluorometer (HORIBA Scientific), respectively.

Spectroelectrochemistry: Tetrahydrofuran (THF) was dried either with activated molecular sieves or with sodium metal and benzophenone. This was distilled and stored under nitrogen. Tetrabutylammonium hexafluorophosphate ($TBAPF_6$) was recrystallized twice from ethanol and dried under vacuum. A honeycomb spectroelectrochemical cell from Pine Research Instruments was used for SEC measurements. Such electrodes have been used for spectroelectrochemical studies of small molecules as well as nanosized carbon dots.[39,40] This system consists of a three-electrode assembly with a transparent gold mesh as the working electrode (WE), gold as a counter electrode (CE) and silver wire as a quasi-reference electrode (QRE). The gold mesh working electrode consists of 19 cylindrical holes. The interior part of each cylinder is also coated with gold. The length and diameter of each cylinder is 1.7 mm and 0.5 mm respectively (See Figure S1). The Ag QRE electrode was calibrated with the ferrocene/ferrocenium couple in THF. The cylindrical geometry of the working electrode offered faster electrolysis times and smaller working volumes than many other SEC systems.[41] A quartz cuvette with an optical pathlength that matched the thickness of the working electrode was used. This enables complete electrolysis of the nanocrystals in the cuvette. All quantum dot samples in this study were dispersed in 0.1 M $TBAPF_6$-THF electrolyte solution. The electrode setup was inserted through a teflon cap into a custom made cuvette of pathlength 1.8 mm. This was sealed with quick melt polymer after filling it with the QD electrolyte solution inside a nitrogen filled glovebox, to avoid contamination

with O_2 and water. Potential and current measurements were carried out using a Metrohm Autolab PGSTAT302 potentiostat. Time-resolved absorption spectra were collected using an Ocean Optics spectrometer equipped with a DH 2000 BAL light source and a USB 2000 VIS-NIR spectrometer. To probe the PL of QD reduced inside the cylindrical electrode, the sample was excited with a 400 nm CW laser and the emission was collected in a 180^o configuration. A long pass filter was used to block the excitation light.

3. Results

3a. Calibration of SEC electrode: The SEC electrode system was calibrated using the ferrocene/ferrocenium couple (See Figure S2). This system yielded a redox potential of 0.150 V vs Ag QRE. Literature gives 0.440 V vs SCE in THF. Hence to obtain values vs the calomel reference, we have used $E_{SCE} = E_{meas} + 0.290V$. The chronoamperometric data of 2 mM $K_3[Fe(CN)_6]$ in 1M KNO_3 was used to extract the effective surface area of the gold mesh using the Cottrell equation. We found a value of 0.48 cm^2 very close to the geometric area of 0.50 cm^2 (see SI.) The initial open circuit potential of the QD solution in de-aerated THF was close to 0 V vs the Ag^+/Ag QRE.

3b. Spectral responses upon charging and discharging: Upon application of a cathodic potential step to -1.8 V, the absorbance of the CdSe QD (d = 5.24 nm, λ_{abs} = 614 nm) solution began to change immediately as shown in Figure 1a, where the absorbance at 614 nm corresponding to the first exciton transition is shown. The exciton band undergoes strong bleaching. Typically it took around 600 seconds for the absorbance to plateau at a new value. This figure also shows that when the potential step was changed from -1.8 V back to 0 V, the absorption signal immediately began to recover. Notably, the recovery step was often faster than the initial absorption changes. Both increases in absorption as well as bleaching were observed but all time traces showed the same kinetics. The recovery

of the absorption spectrum was faster in the first 100 s and more than 90% of the initial absorbance of all bleached peaks had recovered at this point. Importantly, the absorbance always recovered completely, indicating that electrochemical changes were reversible over these timescales.

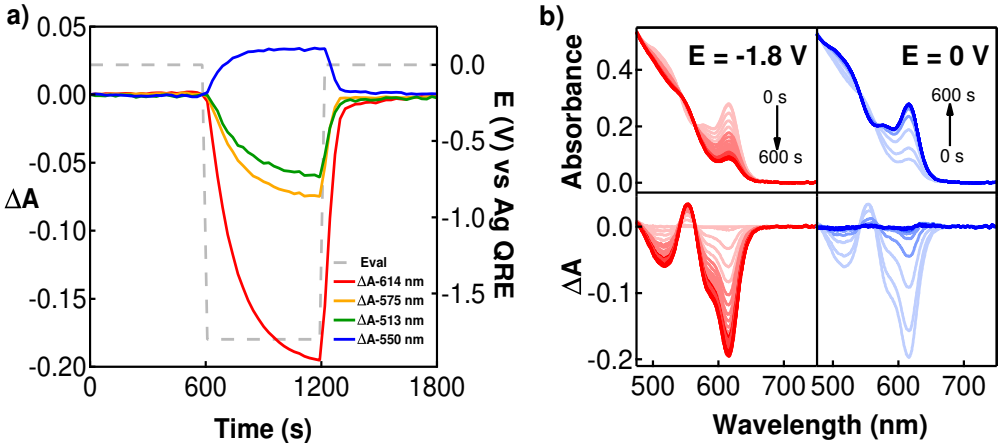

Figure 1: (a) Bleach profile of absorption peaks of CdSe QD capped with oleate ligands (d = 5.24 nm, λ_{abs} = 614 nm) during the entire time duration (1200 s) of a double potential step. The black dotted line indicate the corresponding potential step. Duration of each step (τ) was 600 s. Solution conditions: The QD was dispersed in 0.1 M $TBAPF_6$ in dried and de-aerated THF with OD at exciton peak equal to 0.27. This corresponds to a concentration of 2.5 μM of QD in electrolyte solution. The WE and CE were gold electrodes and a Ag wire was used as QRE. (b) The entire absorbance spectra (upper panel) and corresponding difference spectra (lower panel) of the same QD measured during a double potential step of -1.8 V (red traces) and 0 V (blue traces)vs Ag QRE.

Time dependent spectra collected during cathodic charging to -1.8V and during the subsequent discharge at 0V are presented in Figure 1b. When the -1.8 V potential step was applied, bleaching occurred in the absorption spectra, with peaks at 614 nm, 575 nm, and 513 nm. A new absorption peak evolved at 550 nm and 3 isosbestic points were observed at 563 nm, 542 nm, and 480 nm. There was no evidence for new peaks below the first exciton peak or for red-shifts in the absorption spectrum.

Similar changes in the absorption spectra were observed when the QDs were subjected to a potential sweep measurement (See Figure S5a). The magnitude of the absorbance changes

was lower compared to those obtained during the potential step experiments due to the faster timescales involved. Figure 2a shows the exciton bleach of QD ($d = 3.94$ nm) measured during linear sweep voltammetry (LSV) from 0 V to -2 V at different electrode scan rates (ν). The absorption spectra exhibited no change below -1.5 V. Above this potential (i.e. at more negative potentials), the absorption spectra started to bleach. The onset potential for the bleach was independent of the scan rate. However, the bleach at lower scan rates was larger than that at higher scan rates.

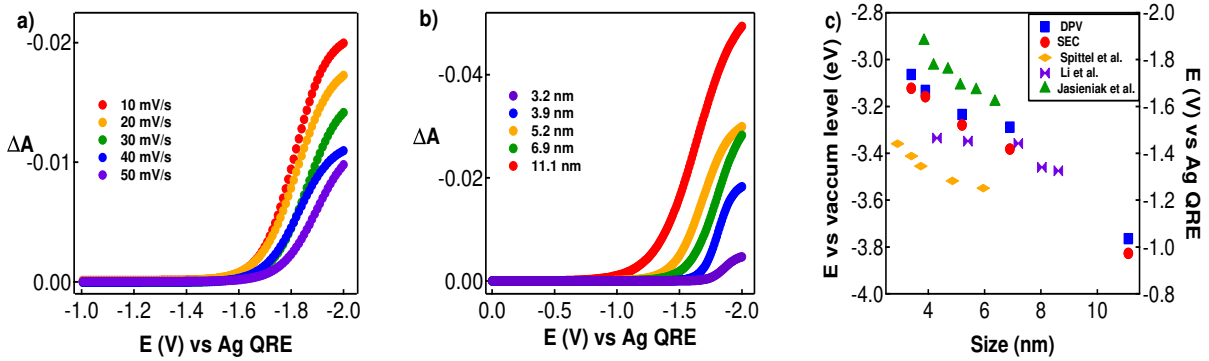

Figure 2: (a) Exciton bleach obtained during LSV of QD ($d = 3.94$ nm, $\lambda_{abs} = 580$ nm) at various scan rates. The region of the bleach profile from 0V to -1V is omitted for clarity (b) Bleach profile of the exciton peak of QDs of different size during the linear potential sweep from 0 V to -2 V at a scan rate $\nu = 10$ mV/s. The solution conditions for both measurements were the same in Figure 1 except the OD at exciton peak was 0.15. (c) Conduction band potential obtained using SEC and DPV was plotted against absolute scale and Ag QRE potential. These values were compared with different experimental values reported in the literature.[35,42,43]

The potential at which bleaching of the CdSe exciton peak started depended on the particle size, as shown in Figure 2b. Larger QDs underwent bleaching at less cathodic potentials than smaller QDs. In these experiments, the absorption at the exciton peak was always 0.15. Note this means the particle concentration was higher for the smaller QDs. Nevertheless, a more negative potential was still required to induce bleaching of the same magnitude. Furthermore, the magnitude of the bleach was higher in larger QDs compared to smaller QDs. In the case of the largest QDs studied with a diameter of 11.1 nm, the bleach almost saturated at -2.0 V but for smaller QDs, the bleach would have required even

more cathodic potentials. By fitting the bleach profile, the onset potential for bleaching of different sized QDs was determined. The bleach profile was fitted using two separate, straight lines: one for the baseline and the other for the rising part of the bleach profile. The intersection point of these straight lines was taken as the reduction potential of the QD (See Figure S5b).[44]

Unfortunately, although the spectroscopic changes suggested that electron transfer was reversible, the corresponding voltammograms exhibited eitherno peaks at all or there were multiple, poorly defined peaks (see Figure S4a). In order to measure the charge transfer to the conduction band states more accurately, differential pulse voltammetry (DPV) was employed. Broad but distinct peaks were observed during the scans (See Figure S4b & c). During anodic scans, the peaks were even broader than those obtained during cathodic scans and these were often limited by the electrochemical window of the electrolyte system. The DPV scans were sensitive to the history of the sample and this resulted in less intense peaks during multiple scans. The conduction band potentials estimated using both SEC and DPV are plotted in Figure 2c. The values show good agreement with those reported in the literature.[35,42,43]

The SEC system was placed on an optical table and the QD photoluminescence was then measured during electrochemical cycling. The set-up enabled both the PL spectra and the relative intensity to be obtained. Figure 3a shows the quenching of the PL of QD (d = 5.24 nm, λ_{abs} = 614 nm, λ_{em} = 624 nm) during a cathodic potential sweep (red traces) and its recovery after a potential step to 0 V was applied for 200 s (blue traces). During the cathodic linear sweep, the PL started to decrease once the potential was below -1.5 V and the initial PL signal was quenched by more than 75% by the end of the sweep. The recovery upon applying a potential step to 0 V was slow compared to the PL quenching and only 30% of the initial value was recovered after 200 s. The exciton absorption bleaching and PL

quenching of QD (d = 5.24 nm) during the LSV are plotted in Figure 3b. From the plot, it clear that the photoluminescence began to be quenched at a less negative potential than the absorption spectra. This suggested that electron transfer occurs at potentials more positive than those leading to exciton bleaching. PL quenching was probed for different sized QDs as well as shelled QDs during potential sweeps. For all the QDs, irrespective of the size or shells, PL quenching began at around -0.5 V (See Figure S8).

Figure 3c presents the recovery dynamics of the exciton bleach from -2V to different cathodic electrode potentials. The QDs were firstly subjected to a linear potential sweep from 0 to -2 V at a scan rate of 10 mV/s to inject electrons. A second potential step to various more positive values, (E_{rec}), was then applied for 100 s (See Figure S10a). For the case where E_{rec} = 0 V, almost 90% of the exciton bleach recovered within 10 s and complete recovery was observed within 100 s. A similar quantitative recovery was observed at -0.2 V. Setting E_{rec} to more negative values slowed down the bleach recovery. When E_{rec} was set to -0.4 V, only 80% of the bleach was recovered within 100 s. On applying -0.6 V and -0.8 V, around 36% and 18% of the initial exciton state absorption had recovered after 100 s respectively.

Figure 3d shows the quenching and recovery of the PL in core and core-shell QDs in response to a potential sweep-step measurement. A similar potential sequence was applied to the experiments in Figure 3c except that E_{rec} was held at 0 V for a duration of 400 s. Following the LSV, the emission intensity was reduced. The CdSe core QDs showed the largest reduction in PL with only 25% of the initial PL retained at the end of the LSV excursion to -2V. The PL increased to a value corresponding to 40% of the initial value on stepping the applied potential back to 0 V. In the case of CdSe/CdS core-shell QDs, 30% of the initial PL intensity was retained at -2V and this increased to 70% upon stepping the potential back to 0 V. For ZnS coated particles, around 36% of PL intensity was retained following electron injection and more than 80% of the PL intensity had recovered by the end of 400 s.

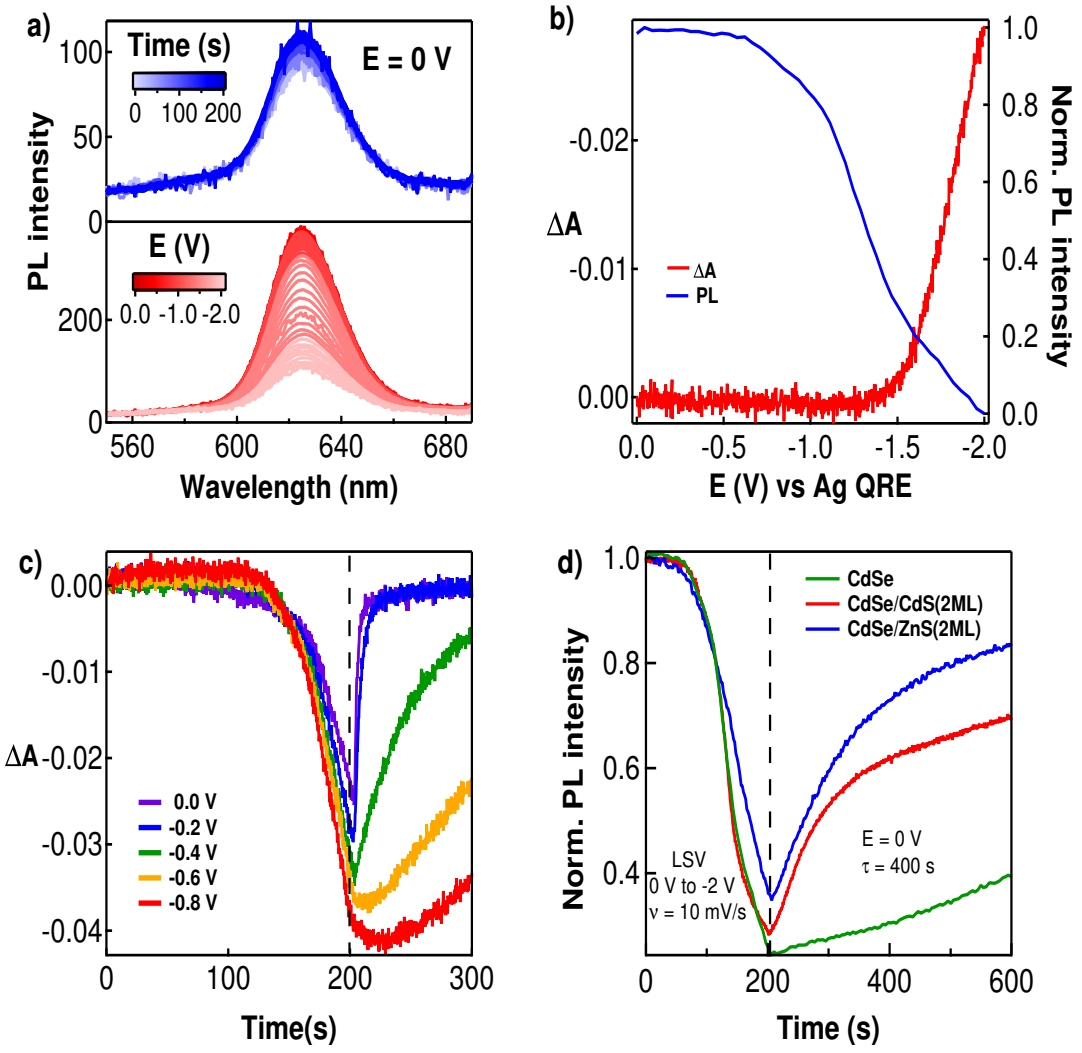

Figure 3: (a) (red trace): The PL measured during LSV of CdSe QD ($d = 5.24$ nm, $\lambda_{abs} = 614$ nm, $\lambda_{em} = 624$ nm) from 0V to -2V; (blue trace): PL of the same QDs when the potential step was re-set to 0 V for 200 s. (b) A comparison of the change in exciton absorption and PL of the same CdSe QD during a potential sweep from 0 V to -2 V. (c) The change in the exciton absorbance during electron injection and its recovery at different potentials. A linear potential sweep from 0 V to -2 V was applied to inject electrons ($\nu = 10$ mV/s). This was followed by a potential step to different values (E_{rec}) for a duration of 100 s to study the influence of electrode potential on the recovery of electrons injected into the exciton states. (d) The change in the PL emission intensity of CdSe (Green curve), CdSe/CdS (Red curve) and CdSe/ZnS (Blue curve) in response to a similar potential sequence except the duration of E_{rec} was 400 s. The core-shell particles were coated with octanethiol and oleic acid. The solution conditions in all these measurements were similar to the condition described in Figure 2

The data above indicated that there were two types of electron transfer. At high cathodic bias, injected electrons were transferred from the electrode directly into the exciton state, leading to bleaching of that transition. However at much lower potentials electrons were still injected. These did not lead to direct bleaching of the exciton absorption on these time scales but they did quench the PL. These electrons must have been transferred into surface traps. They did not seem to transfer back to the electrode as quickly as electrons in the exciton states. The rate of recovery and the degree of recovery was also affected by the presence of shell layers on the QD. This suggested that trap states figured prominently in the "sub-exciton" electron injection.

3c. Chronoamperometry of CdSe QDs: To explore the electron injection at "sub-bandgap potentials", potential steps of varying duration were applied to QDs with four different surface modifications. For the first sample, we used QDs with the standard oleate capping. For the second sample, we replaced the oleate ions by addition of trioctylphosphine (TOP). In the third and fourth samples, we used CdS and ZnS as shell layers respectively. Figure 4a shows the applied potential step sequence (black trace) from 0V to -2V (vs Ag QRE) and the resulting bleach profiles for QDs with three different sizes, all coated with oleate ions. Here an "injection potential step" and "recovery potential step" were applied alternately. The duration of each potential step, called τ hereafter, was 100 s. The rest of the traces in Figure 4a comprise the exciton bleach profiles for three, differently sized, oleate capped QDs in response to the potential steps. As with the sweep measurements, the QDs exhibited a size-dependent response with larger QDs bleaching at lower potentials and exhibiting larger bleaches.

CdSe QDs ($d = 5.24$ nm, $\lambda_{abs} = 614$ nm) were used for the ligand exchange and shelling. In this way, the responses obtained for both ligand exchanged and shelled QDs could be directly compared to the responses from the parent, oleate capped QDs. Figure 4b shows the bleach profile of CdSe QDs capped with cadmium oleate and after exchange with trioctylphosphine (TOP). After exchange, there was no change in the absorption spectrum (See

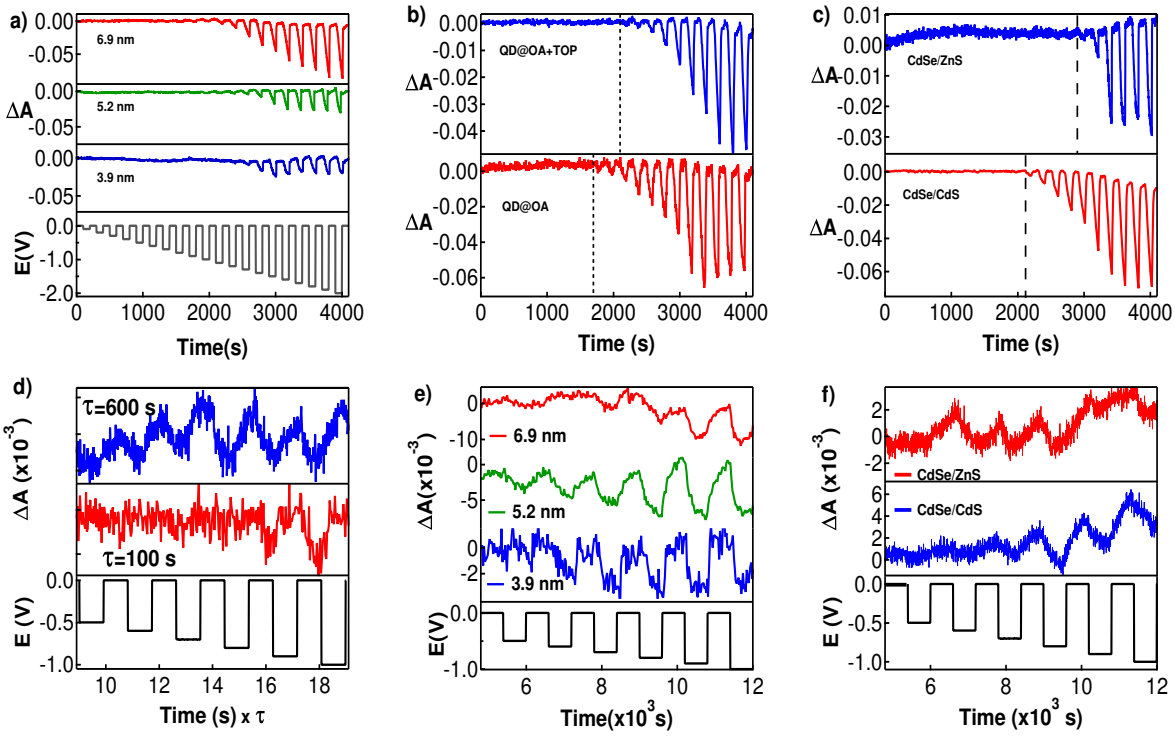

Figure 4: (a) Exciton bleach profile of CdSe QD with three different sizes: 6.90 nm (blue), 5.24 nm (green) and 3.94 nm (red) in response to the potentials steps illustrated in black. The QDs were capped with oleate ions. The duration of each step (τ) is 100 s. (b) Exciton peak bleach profile of CdSe QD coated Cd-oleate and TOP (d = 5.24 nm). (c) Exciton peak bleach profile of CdSe/CdS and CdSe/ZnS. The dotted line indicates the onset of bleach. (d) Exciton absorbance bleach of QD (d = 5.24 nm) when potential step duration τ is varied. The black trace shows the applied potential. The red trace corresponds to the bleach when τ = 100 s and blue trace to the bleach signal when τ = 600 s. (e) Bleaching of QDs with three different sizes at low potentials when τ = 600 s. There was no strict size dependence compared to the bleaching of exciton peak when τ = 100 s. (f) Absorbance bleach for CdSe/CdS (blue trace) and CdSe/ZnS (red trace) when the τ was 600 s. The solution conditions were the same as those in Figure 2

Figure S3a).[45] However, when the QDs were subjected to the same potential step, the bleach started at 300 mV above the onset bleach potential for oleate capped QDs. The black dotted line in Figure 4b shows the extrapolated potential for the onset of the bleach signal. The magnitude of the bleach was also reduced with TOP.

To further test the effect of inorganic passivation on the electron injection, the QDs were shelled with 2 monolayers of CdS and ZnS. Coating with CdS led to a red-shift of the first exciton peak by 10 nm, while there was a blue-shift of 8 nm when the QD was coated with ZnS (See Figure S3b). The bleach profiles of these two types of QDs in response to a potential step ($\tau = 100$ s) are plotted in Figure 4c. It is evident that the potential for onset of the bleaching of the exciton peak in the shelled QDs moved to a higher, more cathodic potential relative to the core CdSe QDs. However, the bleach profiles of these two shelled materials also differed. CdSe/CdS QDs started to bleach at -1.1 V compared to -1.5 V for CdSe/ZnS QDs. Furthermore, the magnitude of the bleach in the case of CdSe/CdS QDs was approximately twice that of the bleach observed for CdSe/ZnS QDs. Bleaching at lower potentials, observed for CdSe cores, was eliminated in ZnS coated particles but not in the case of CdSe/CdS QDs. Bleach features observed with CdSe/CdS QDs were similar to those observed with CdSe QDs, except the induced absorption at 550 nm observed in CdSe was merged with other bleach features in CdSe/CdS spectra. ZnS coated particles were entirely different. They exhibited a new broad peak around 475 nm after electron injection (See Figure S11c & d).

The period of equilibration at each potential was important. When τ was set to 600 s, the onset of the bleach in CdSe QDs ($d = 5.24$ nm) started around -0.5 V as displayed in Figure 4d. The exciton peak also recovered when the potential was stepped back to 0 V. In Figure 4e, similar low potential bleaching when $\tau = 600$ s was found in other QDs and the onset potential of the bleach was similar i.e. -0.5 V. The bleaching was also found to increase with increase in concentration. Unlike the bleaching when τ was 100 s, this bleaching was

present in both CdSe/CdS and CdSe/ZnS (Figure 4f). This indicates that neither the size of the QD nor the surface chemistry influenced the formation of the trion state at when τ was long enough.

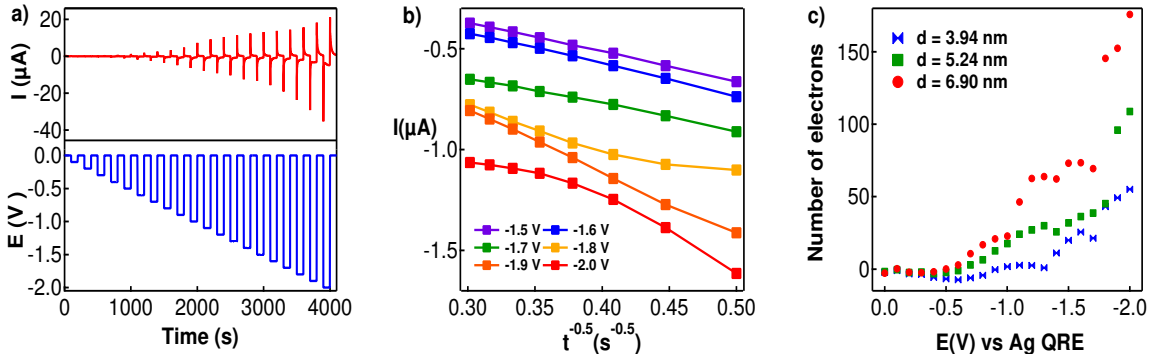

Figure 5: I-V data collected during CdSe QD electrochemistry (d = 5.24 nm, λ_{abs} = 614 nm).[CdSe] = 1.46 μM. The solution conditions were the same as in Figure 2. (a) Measured current (red) at the gold mesh working electrode during a series of potential steps (blue). (b) Cottrell plot of the current vs $t^{-0.5}$ at different potential steps. The plot shows the cathodic current measured during intermediate time scales of potential step. The total duration of each step (τ) was 100 s . (c) The number of electrons injected at different cathodic potential step for QDs of three different size estimated using the Cottrell equation.

Figure 5a shows the background subtracted current resulting from the potential step (τ=100 s) described above. The reference was the same solvent and electrolyte but in the absence of the CdSe QDs. A negative current was recorded when an injection potential was applied and a positive current was measured when the potential was stepped back to 0 V. As the potential step was raised, the resulting current also increased but the magnitude of the cathodic current was always larger than the anodic current when the potential was stepped back to 0V. The current was found to be proportional to the inverse square root of time ($\sqrt{1/t}$) (See Figure 5b), which suggests the Cottrell equation may be applicable. Integration of the Cottrell equation was used to determine the number of electrons injected. Unlike normal molecular redox chemistry, this number was not fixed but was a function of potential. The number of electrons injected into QDs of different sizes during the cathodic potential steps is shown in Figure 5c. Up to 150 electrons were injected at high cathodic bias and the number

increased with QD size. It should be also noted that the potential onset for electron transfer in all QDs occurred at $\sim$ -0.5 V.

4. Discussion

The results presented here clearly demonstrate that: (i) electrons can be facilely transferred into CdSe QDs in solution from a gold electrode in THF and that they can also be quickly extracted. As a result the degree of exciton bleaching and its recovery can be controlled through the applied potential; (ii) the injection potential depends on particle size but not the scan rate; (iii) the PL is quenched by electron injection but not completely. Furthermore, quenching begins at potentials below where electrons are injected into the exciton states. PL quenching is therefore due to electrons in surface traps; (iv) although significant number of electrons are transferred to each particle, only those injected into the $1S_e$ state strongly bleach the absorption spectrum of the QD.

The data have been collected using a honeycomb mesh electrode and it is worth considering the role of the electrode. We note first of all that there are two time constants in the cylindrical SEC geometry. At short times, QDs within the cylindrical pores diffuse to the gold mesh and undertake electron transfer. At much longer times, QDs diffuse from the reservoir to the mesh. The data up to 600 seconds here are primarily due to QDs reacting within the pores.[41] This geometry allows analytical equations to be applied to the current-time response as shown in the SI and elsewhere.[41,46] A wide electrochemical window is obtained by dispersing the QDs in THF and using $TBAPF_6$ as electrolyte. However, this places some limits on the stabilizers used to prevent colloid aggregation. The ligands must provide a strong steric barrier and also must be able to prevent "salting out" at the high ionic strength used. As a result, long chain surfactants are needed. This in turn means that electrons are transferred through surfactant molecules coating the gold electrode and also

around the QDs. Hence electrons effectively tunnel through a low dielectric bilayer. The blank electrolyte itself does not exhibit any changes in absorbance in response to applied potentials. In order to avoid the intercalation of metal ions into the QD lattice at negative potentials, electrolytes containing bulky organic ions have been used.[47]

4a. Spectroelectrochemistry of CdSe QD in solution: The spectroelectrochemical changes observed and described in section 3b show some parallels to those observed during spectroelectrochemistry of CdSe QD films but there are also key differences.[48] Bleaching of the absorption spectra in response to the cathodic bias results from the injection of electrons into the conduction band or exciton state of the QD. The bleach features are similar to those reported in the literature.[13,32,35] However no red-shift of the spectrum is observed. This is usually attributed to a Stark effect on the exciton state in thin film SEC. Nevertheless large numbers of electrons are injected. Hence in solution phase SEC, the Stark effect must be reduced due to strong cation binding to the QD in response to electron transfer.[48] The bleach at 614 nm and 575 nm in Figure 1b can be correlated to the occupation of $1S_e$ states and thus blocking the $1S_{3/2h}$-$1S_e$ and $2S_{3/2h}$-$1S_e$ transitions respectively. The appearance of a new peak at 550 nm can be attributed to an induced absorption as a result of charging the QD.[49,50] The bleach feature at 513 nm is assigned to the blocking of the $1P_{3/2h}$-$1P_e$ transition. The kinetics of charging and discharging of QD exciton states can be extracted from the time-resolved absorption spectra measured during the potential steps if one assumes that the bleach is linear with the probability of occupation. The bleach and recovery of absorption spectra during these measurement are comparable to those observed in thin film SEC.

Even after multiple electrochemical cycles (for over 100 mins.) of the potential between -1.5 V and 0 V with $\tau = 600$ s, no blue shift, loss of absorbance or evidence for QD aggregation is observed. These observations highlight the excellent colloidal stability of QDs reduced using solution phase SEC and show that electron transfer is highly reversible and does not lead to cathodic dissolution, i.e. the negative trion state is quite stable in nitrogen saturated THF. However we do note that the exciton bleach does increase with cycling, as shown in

(See Figure S6). The reasons for this have not been explored.

The magnitude of the exciton peak bleach signal is affected by the scan rate. In Figure 2a, the onset of the bleach signal starts more or less at the same potential but slower scan rates results in bigger bleach signals. An inverse relationship is observed between the scan rate and the magnitude of the bleach signal in contrast to the square-root scan rate ($\sqrt{\nu}$) dependence predicted by the Randles-Sevcik equation. However, this behaviour is in accordance with the trend observed in molecular SEC where absorbance changes are found to be directly proportional to the charge transferred and inversely proportional to the scan rate.[51] Hence slow scan rates are preferable for obtaining the maximum optical response and therefore all the sweep measurements have been carried out at $\nu = 10$ mV/s.

4b. Determination of conduction band edge potentials: Bleaching of exciton peaks in response to a potential sweep is often exploited to estimate the reduction potentials of QDs because well-defined voltammetric peaks are difficult to observe during QD CV.[17,20,21] The onset potential for bleaching can be correlated to the reduction potential of QDs or the position of the $1S_e$ state since bleaching of the exciton peak should begin when the electrode Fermi level lies close to this level. The reduction potential of QDs of various sizes has been extracted from the potential at the onset of bleaching by fitting the bleach profile.[44] DPV measurements are reported to provide a better estimate of the redox potentials of QDs, because it is difficult to measure significant Faradaic current against the background current during LSV.[52] We still observe multiple peaks during DPV (Figure S4b & c). Even so sensible values for the $1S_e$ energy level can be gleaned, as shown in Figure 2c. Band edge potentials from literature are compared here and these have been determined by different methods including: SEC on CdSe QD films coated with alkylthiols,[35] PESA on QD capped with TOPO[42] and CV of CdSe QDs passivated with carboxylate ions and TOPO.[43] More accurate values might be possible once the ligand chemistry can be accounted for. Our measurements are in good agreement with the pseudopotential calculations of Jasieniak et al.[42] and we conclude that SEC is a useful method for measuring the energy levels of QDs.

4c. Stability of excess electrons in conduction band: As shown in Figure 1, there is strong bleaching of the exciton state upon electron injection. The bleach signal is stable for hours provided the electrode is maintained at this potential. If the electrode is stepped to a more positive potential, the electrons are re-extracted. The rate and degree of extraction strongly both depend on the electrode potential, as shown in Figure 3c and Figure S10b & c). This does not prove unambiguously that the injected electrons reside continuously in the $1S_e$ state. If they relax into trap states, the QD could pick up a further electron from the electrode. However, such a relaxation process would necessarily be slow since it takes some 600 seconds for all the QDs in the optical pathway to diffuse to the electrode. Significantly, even after a long period at -1.8 V, the electrons are rapidly extracted if the potential is stepped to 0V vs QRE. For intermediate potentials, the bleach signal recovers more slowly, showing that there is a kinetic barrier to back electron transfer, as seen in Figure 3c. The rate of back transfer also depends on the QD size, with smaller particles exhibiting faster bleach recovery. Similar potential dependent recovery profiles were obtained for other QDs of different sizes (See Figure S10b & c). A similar slow recovery of the exciton bleach has also been reported for photodoped and chemically reduced CdSe nanocrystals, which was attributed to midgap electron traps.[26,53]

The PL quenching is very sensitive to electron injection and quenching begins at much more positive potentials compared to the absorbance bleaching as shown in Figure 3b. In the case of QDs of size 5.24 nm, the absorbance starts to bleach at -1.5 V whereas the onset of PL quench starts at around -0.5 V. This demonstrates that (i) unoccupied surface states do exist on the QD; (ii) direct electron transfer into these surface states can occur and (iii) such injected electrons interact with excitons, reducing radiative recombination, compared to the uncharged state. The slow recovery of PL, as shown in Figure 3a, indicates there is a high activation barrier for back transfer. This was in contrast to the PL recovery kinetics observed during thin film SEC.[54]

In the presence of a CdS or ZnS shell, the number of trap states is reduced, as evident from

the smaller PL loss during cathodic sweeps. The PL also recovers to a greater extent although it still lags the recovery in absorption. This shows that these shells reduce the number of surface traps. However the PL does begin to decrease at the same potential, irrespective of the ligand (oleate or TOP) or the presence of a shell, at around -0.5V. This is in contrast to the recent results published by Houtepen et al., who observed a shift in the potential for onset of PL quenching in CdSe/CdS QD films with different shell thickness during potential sweeps.[55] However, the dramatic increase in the recovery rate for shelled particles compared to the core can be attributed to the elimination of traps which are responsible for the trapping of electrons injected. Our result shows that ZnS shells are better at eliminating such traps.

4d. Kinetics of Electron Transfer: The number of electrons injected into the exciton state of QDs is usually derived from the exciton absorption bleach. Since the degeneracy of this state is 2, injecting two electrons should in principle completely bleach the absorption peak. For example, from the bleach and recovery profile of QD shown in Figure 1a, we have calculated the number of electrons injecting into the QD. We find that a maximum of 1.4 electrons are injected at the end of a cathodic potential step of -1.8 V. All of these electrons are extracted back from the CB upon reversing the potential (See Figure S7a).

However, the current measurements carried out here (see Figure 5a) indicate that far more electrons are injected and as we show below, Fermi level equilibration requires far more than 2 electrons. We find that the cathodic injection current is always higher than the recovery (anodic) current. This implies there is hysteresis associated with electron transfer between the electrode and surface states, even though there is faster, reversible transfer between the $1S_e$ state and the electrode.

Electron transfer is therefore complex. Even in the absence of stray background currents, there is the double layer charging current for the electrode and the QD itself has a double layer capacitance. As the gold electrode is ramped to more negative potentials, the driving force for electron transfer increases and should become diffusion limited. However, unlike reduction of say ferricyanide ions, where the number of electrons is fixed at n=1, here the

number being transferred is a strong function of the applied potential. We find that the Cottrell equation is obeyed even though the current is still rising and is potential dependent. This seems contradictory but we believe this reflects the fact that even during diffusion-limited, Brownian encounters with the electrode, the number of electrons being transferred depends on the number of surface states available.

The linearity of current vs $\sqrt{1/t}$ plot demonstrates that the electron transfer is diffusion controlled. In the diffusion-limited region, the measured current (i_d) can be related to the time (t) and the number of electrons injected (n) through the Cottrell equation (modified for cylindrical electrodes):[41,46]

$$i_d = nFAC\left(\sqrt{\frac{D}{\pi t}} + \frac{D}{2r}\right)$$

where F is the Faraday constant, A is the effective electrochemical surface area, D is the diffusion coefficient, C is the initial concentration and$r$ is the radius of the cylinder. The linear portion of the i_d vs $\sqrt{1/t}$ plot at intermediate timescales is selected for fitting to avoid the contribution of non-Faradaic current at short time scales and the effects of planar diffusion at longer time scales (See Supporting information for details).

From the slope of i_d vs $\sqrt{1/t}$, the number of electrons injected into the QD can be calculated. We consistently find that the Cottrell equation cedes numbers up to 150 at high negative biasses. Two different trials of QDs of the same size as well as experiments at two different concentrations have yielded similar numbers (See Figure S7b). Such large electron counts have been previously reported in nanocrystals. In the cases of colloidal silver and colloidal gold nanoparticles, thousands of electrons are injected per particle.[30,31] Bard et al. has estimated the passage of around 50 electrons at redox peak potentials in CdS QDs.[56,57] Another calculation using electrochemical measurements on CdS has also yielded electron counts in the hundreds.[57] By correlating the broad band edge tail in the absorbance of chemically reduced CdSe to the electron present in surface states,around 8-10

electrons have been estimated to reside in surface states.[11] A recent calculation based on titration of chemically reduced CdSe QDs (with a similar surface chemistry to that used in our experiments) yielded around 50 electrons localised on surface states.[26] Hence these numbers seem consistent with other studies.

Finally, if we assume that a QD in 0.1 M electrolyte is a spherical capacitor and the double layer capacitance is controlled by a Helmholtz layer whose thickness is determined by the length of the C18 chains on the capping ligands, then typical values would be of order K = 20 μF cm^{-2}. To charge this double layer from 0V to -1V would require of order Q = K * V = 140 electrons for a QD with radius 3 nm. The TBA+ ions would act as the counterions at the outer Helmholtz plane. This suggests it is not unreasonable to have more than 100 electrons transferring during encounters with the gold electrode. However, it is surprising that these charges do not have more impact on the exciton transition.

4e. The Role of Ligands: In order to investigate the influence of surface species the surface chemistry can be altered. The bleach profile of TOP passivated QDs (τ = 100 s) varies significantly from that obtained from the parent QD. From the absorption spectra of these particles, it is evident that the TOP is not electronically interacting with the exciton states since the position of exciton peak before and after ligand exchange is identical. Hence the shift in the onset potential of bleach as well as reduction in its intensity observed after TOP passivation can be only attributed to the change in surface chemistry. Anderson et al. have reported the displacement of Z type ligands from the surface of QD with L type ligands.[45] Here a similar mechanism is postulated, i.e. the cadmium oleate ions are replaced by alkylphosphine molecules, thereby reducing the concentration of surface Cd sites but increasing the concentration of exposed Se sites. The QD surface chemistry shifts from being 'Cd rich' to 'Se rich'.[58] Since Cd 5s orbitals are the likely source of electron accepting surface states, TOP can reduce their concentration, and push the onset for electron transfer to more negative potentials. In the case of shelled QDs, the ZnS reduces the current significantly compared to the core CdSe QDs. The surface zinc ions are poorer electron acceptors than Cd

ions. However, we cannot exclude the possibility that the injected electrons are also reducing oxidized surface selenium sites. Tsui et al. injected electrons using photodoping and they suggested that the reduction of surface chalcogenide species is responsible for photodoping.[27] Jha and Guyot-Sionnest also proposed that the PL quenching might be due to the reduction of oxidized selenium species.[54]

Conclusions

We have undertaken spectroelectrochemistry of CdSe QDs dispersed in THF. The SEC absorption data are similar and comparable to those obtained from thin film SEC except for those influenced by interparticle interactions. From the bleach profile of QDs, the conduction band potentials have been determined. The decay kinetics of injected electrons from the CB of QDs are found to be potential dependent. Calculations based on chronoamperometric measurement indicate the passage of ten to hundred fifty electrons into the QD, depending on the applied potential and size of the QD. Two different types of trap activation have been found during the application of potential steps. This is supported by the bleaching of absorption, PL quenching and the transfer of electrons at potentials well below the conduction band edge. By manipulating the surface chemistry of QD in these experiments, we rationalise that this current results in reduction of surface cadmium and chalcogenide species. Remarkably we find the negative trion state is stable for hours and that the excess electrons can be readily extracted.

References

(1) Zhu, H.; Yang, Y.; Wu, K.; Lian, T. Charge Transfer Dynamics from Photoexcited Semiconductor Quantum Dots. *Annual Review of Physical Chemistry* **2016**, *67*, 259–281.

(2) Zhao, J.; Holmes, M. A.; Osterloh, F. E. Quantum Confinement Controls Photocatalysis: A Free Energy Analysis for Photocatalytic Proton Reduction at CdSe Nanocrystals. *ACS Nano* **2013**, *7*, 4316–4325.

(3) Wang, J.; Ding, T.; Wu, K. Charge Transfer from n-Doped Nanocrystals: Mimicking Intermediate Events in Multielectron Photocatalysis. *Journal of the American Chemical Society* **2018**, *140*, 7791–7794.

(4) Hu, Z.; Liu, S.; Qin, H.; Zhou, J.; Peng, X. Oxygen Stabilizes Photoluminescence of CdSe/CdS Core/Shell Quantum Dots via Deionization. *Journal of the American Chemical Society* **2020**, *142*, 4254–4264.

(5) Haase, M.; Weller, H.; Henglein, A. Photochemistry and radiation chemistry of colloidal semiconductors. 23. Electron storage on zinc oxide particles and size quantization. *The Journal of Physical Chemistry* **1988**, *92*, 482–487.

(6) Cohn, A. W.; Janßen, N.; Mayer, J. M.; Gamelin, D. R. Photocharging ZnO nanocrystals: picosecond hole capture, electron accumulation, and auger recombination. *The Journal of Physical Chemistry C* **2012**, *116*, 20633–20642.

(7) Tvrdy, K.; Kamat, P. V. Substrate Driven Photochemistry of CdSe Quantum Dot Films: Charge Injection and Irreversible Transformations on Oxide Surfaces. *The Journal of Physical Chemistry A* **2009**, *113*, 3765–3772.

(8) Nirmal, M.; Dabbousi, B. O.; Bawendi, M. G.; Macklin, J. J.; Trautman, J. K.; Harris, T. D.; Brus, L. E. Fluorescence intermittency in single cadmium selenide nanocrystals. *Nature* **1996**, *383*, 802–804.

(9) Saba, M.; Aresti, M.; Quochi, F.; Marceddu, M.; Loi, M. A.; Huang, J.; Talapin, D. V.; Mura, A.; Bongiovanni, G. Light-Induced Charged and Trap States in Colloidal Nanocrystals Detected by Variable Pulse Rate Photoluminescence Spectroscopy. *ACS Nano* **2013**, *7*, 229–238.

(10) Shim, M.; Guyot-Sionnest, P. n-type colloidal semiconductor nanocrystals. *Nature* **2000**, *407*, 981–983.

(11) Shim, M.; Wang, C.; Guyot-Sionnest, P. Charge-tunable optical properties in colloidal semiconductor nanocrystals. *The Journal of Physical Chemistry B* **2001**, *105*, 2369–2373.

(12) Yu, D.; Wang, C.; Guyot-Sionnest, P. n-Type conducting CdSe nanocrystal solids. *Science* **2003**, *300*, 1277–1280.

(13) Rinehart, J. D.; Schimpf, A. M.; Weaver, A. L.; Cohn, A. W.; Gamelin, D. R. Photochemical electronic doping of colloidal CdSe nanocrystals. *Journal of the American Chemical Society* **2013**, *135*, 18782–18785.

(14) Guyot-Sionnest, P.; Wang, C. Fast voltammetric and electrochromic response of semiconductor nanocrystal thin films. *The Journal of Physical Chemistry B* **2003**, *107*, 7355–7359.

(15) Boehme, S. C.; Wang, H.; Siebbeles, L. D. A.; Vanmaekelbergh, D.; Houtepen, A. J. Electrochemical charging of CdSe quantum dot films: dependence on void size and counterion proximity. *ACS nano* **2013**, *7*, 2500–2508.

(16) Gudjonsdottir, S.; van der Stam, W.; Kirkwood, N.; Evers, W. H.; Houtepen, A. J. The Role of Dopant Ions on Charge Injection and Transport in Electrochemically Doped Quantum Dot Films. *Journal of the American Chemical Society* **2018**, *140*, 6582–6590.

(17) Inamdar, S. N.; Ingole, P. P.; Haram, S. K. Determination of Band Structure Parameters and the Quasi-Particle Gap of CdSe Quantum Dots by Cyclic Voltammetry. *ChemPhysChem* **2008**, *9*, 2574–2579.

(18) Kucur, E.; Bücking, W.; Giernoth, R.; Nann, T. Determination of defect states in

semiconductor nanocrystals by cyclic voltammetry. *The Journal of Physical Chemistry B* **2005**, *109*, 20355–20360.

(19) Ingole, P. P.; Markad, G. B.; Saraf, D.; Tatikondewar, L.; Nene, O.; Kshirsagar, A.; Haram, S. K. Band Gap Bowing at Nanoscale: Investigation of CdS x Se1–x Alloy Quantum Dots through Cyclic Voltammetry and Density Functional Theory. *The Journal of Physical Chemistry C* **2013**, *117*, 7376–7383.

(20) Haram, S. K.; Quinn, B. M.; Bard, A. J. Electrochemistry of CdS Nanoparticles: A Correlation between Optical and Electrochemical Band Gaps. *Journal of the American Chemical Society* **2001**, *123*, 8860–8861.

(21) Myung, N.; Ding, Z.; Bard, A. J. Electrogenerated chemiluminescence of CdSe nanocrystals. *Nano Letters* **2002**, *2*, 1315–1319.

(22) Poznyak, S. K.; Osipovich, N. P.; Shavel, A.; Talapin, D. V.; Gao, M.; Eychmüller, A.; Gaponik, N. Size-dependent electrochemical behavior of thiol-capped CdTe nanocrystals in aqueous solution. *The Journal of Physical Chemistry B* **2005**, *109*, 1094–1100.

(23) Kuçur, E.; Bücking, W.; Arenz, S.; Giernoth, R.; Nann, T. Heterogeneous Charge Transfer of Colloidal Nanocrystals in Ionic Liquids. *ChemPhysChem* **2006**, *7*, 77–81.

(24) Haram, S. K.; Kshirsagar, A.; Gujarathi, Y. D.; Ingole, P. P.; Nene, O. A.; Markad, G. B.; Nanavati, S. P. Quantum confinement in CdTe quantum dots: investigation through cyclic voltammetry supported by density functional theory (DFT). *The Journal of Physical Chemistry C* **2011**, *115*, 6243–6249.

(25) Chen, M.; Guyot-Sionnest, P. Reversible Electrochemistry of Mercury Chalcogenide Colloidal Quantum Dot Films. *ACS Nano* **2017**, *11*, 4165–4173.

(26) Hartley, C. L.; Dempsey, J. L. Electron-promoted X-type ligand displacement at CdSe quantum dot surfaces. *Nano letters* **2019**, *19*, 1151–1157.

(27) Tsui, E. Y.; Hartstein, K. H.; Gamelin, D. R. Selenium redox reactivity on colloidal CdSe quantum dot surfaces. *Journal of the American Chemical Society* **2016**, *138*, 11105–11108.

(28) Houtepen, A. J.; Hens, Z.; Owen, J. S.; Infante, I. On the Origin of Surface Traps in Colloidal II–VI Semiconductor Nanocrystals. *Chemistry of Materials* **2017**, *29*, 752–761.

(29) Du Fossé, I.; Ten Brinck, S.; Infante, I.; Houtepen, A. J. Role of Surface Reduction in the Formation of Traps in n-Doped II–VI Semiconductor Nanocrystals: How to Charge without Reducing the Surface. *Chemistry of Materials* **2019**, *31*, 4575–4583.

(30) Ung, T.; Giersig, M.; Dunstan, D.; Mulvaney, P. Spectroelectrochemistry of Colloidal Silver. *Langmuir* **1997**, *13*, 1773–1782.

(31) Novo, C.; Funston, A. M.; Gooding, A. K.; Mulvaney, P. Electrochemical charging of single gold nanorods. *Journal of the American Chemical Society* **2009**, *131*, 14664–14666.

(32) Wang, C.; Shim, M.; Guyot-Sionnest, P. Electrochromic nanocrystal quantum dots. *Science* **2001**, *291*, 2390–2392.

(33) Galland, C.; Ghosh, Y.; Steinbrück, A.; Sykora, M.; Hollingsworth, J. A.; Klimov, V. I.; Htoon, H. Two types of luminescence blinking revealed by spectroelectrochemistry of single quantum dots. *Nature* **2011**, *479*, 203–207.

(34) Gooding, A. K.; Gómez, D. E.; Mulvaney, P. The effects of electron and hole injection on the photoluminescence of CdSe/CdS/ZnS nanocrystal monolayers. *ACS nano* **2008**, *2*, 669–676.

(35) Spittel, D.; Poppe, J.; Meerbach, C.; Ziegler, C.; Hickey, S. G.; Eychmuller, A. Absolute

energy level positions in CdSe nanostructures from potential-modulated absorption spectroscopy (EMAS). *ACS nano* **2017**, *11*, 12174–12184.

(36) Boehme, S. C.; Vanmaekelbergh, D.; Evers, W. H.; Siebbeles, L. D. A.; Houtepen, A. J. In situ spectroelectrochemical determination of energy levels and energy level offsets in quantum-dot heterojunctions. *The Journal of Physical Chemistry C* **2016**, *120*, 5164–5173.

(37) Jasieniak, J.; Bullen, C.; Van Embden, J.; Mulvaney, P. Phosphine-free synthesis of CdSe nanocrystals. *The Journal of Physical Chemistry B* **2005**, *109*, 20665–20668.

(38) Boldt, K.; Kirkwood, N.; Beane, G. A.; Mulvaney, P. Synthesis of Highly Luminescent and Photo-Stable, Graded Shell CdSe/Cd x Zn1–x S Nanoparticles by In Situ Alloying. *Chemistry of Materials* **2013**, *25*, 4731–4738.

(39) Kellett, C. W.; Swords, W. B.; Turlington, M. D.; Meyer, G. J.; Berlinguette, C. P. Resolving orbital pathways for intermolecular electron transfer. *Nature communications* **2018**, *9*, 1–10.

(40) Liang, Z.; Kang, M.; Payne, G. F.; Wang, X.; Sun, R. Probing energy and electron transfer mechanisms in fluorescence quenching of biomass carbon quantum dots. *ACS applied materials interfaces* **2016**, *8*, 17478–17488.

(41) Porter, M. D.; Kuwana, T. Glassy carbon and graphite electrodes with a hole for long path length thin-layer spectroelectrochemistry. *Analytical Chemistry* **1984**, *56*, 529–534.

(42) Jasieniak, J.; Califano, M.; Watkins, S. E. Size-dependent valence and conduction band-edge energies of semiconductor nanocrystals. *ACS nano* **2011**, *5*, 5888–5902.

(43) Liu, J.; Yang, W.; Li, Y.; Fan, L.; Li, Y. Electrochemical studies of the effects of the

size, ligand and composition on the band structures of CdSe, CdTe and their alloy nanocrystals. *Physical Chemistry Chemical Physics* **2014**, *16*, 4778–4788.

(44) Shallcross, R. C.; Zheng, Y.; Saavedra, S. S.; Armstrong, N. R. Determining Band-Edge Energies and Morphology-Dependent Stability of Formamidinium Lead Perovskite Films Using Spectroelectrochemistry and Photoelectron Spectroscopy. *Journal of the American Chemical Society* **2017**, *139*, 4866–4878.

(45) Anderson, N. C.; Hendricks, M. P.; Choi, J. J.; Owen, J. S. Ligand Exchange and the Stoichiometry of Metal Chalcogenide Nanocrystals: Spectroscopic Observation of Facile Metal-Carboxylate Displacement and Binding. *Journal of the American Chemical Society* **2013**, *135*, 18536–18548.

(46) Bansal, N. P.; Plambeck, J. A. An aid to the interpretation of electrochemical data measured with spherical and cylindrical electrodes: corrections to the Cottrell equation. *Canadian Journal of Chemistry* **1978**, *56*, 155–156.

(47) Puntambekar, A.; Wang, Q.; Miller, L.; Smieszek, N.; Chakrapani, V. Electrochemical charging of CdSe quantum dots: Effects of adsorption versus intercalation. *ACS nano* **2016**, *10*, 10988–10999.

(48) Houtepen, A. J.; Vanmaekelbergh, D. Orbital occupation in electron-charged CdSe quantum-dot solids. *The Journal of Physical Chemistry B* **2005**, *109*, 19634–19642.

(49) Sewall, S. L.; Cooney, R. R.; Anderson, K. E. H.; Dias, E. A.; Sagar, D. M.; Kambhampati, P. State-resolved studies of biexcitons and surface trapping dynamics in semiconductor quantum dots. *The Journal of chemical physics* **2008**, *129*, 084701.

(50) Klimov, V. I. Optical Nonlinearities and Ultrafast Carrier Dynamics in Semiconductor Nanocrystals. *The Journal of Physical Chemistry B* **2000**, *104*, 6112–6123.

(51) Bancroft, E. E.; Sidwell, J. S.; Blount, H. N. Derivative linear sweep and derivative cyclic voltabsorptometry. *Analytical Chemistry* **1981**, *53*, 1390–1394.

(52) Impellizzeri, S.; Monaco, S.; Yildiz, I.; Amelia, M.; Credi, A.; Raymo, F. M. Structural implications on the electrochemical and spectroscopic signature of CdSe-ZnS Core Shell quantum dots. *The Journal of Physical Chemistry C* **2010**, *114*, 7007–7013.

(53) Tsui, E. Y.; Carroll, G. M.; Miller, B.; Marchioro, A.; Gamelin, D. R. Extremely slow spontaneous electron trapping in photodoped n-type CdSe nanocrystals. *Chemistry of Materials* **2017**, *29*, 3754–3762.

(54) Jiha, P. P.; Guyot-Sionnest, P. Photoluminescence switching of charged quantum dot films. *The Journal of Physical Chemistry C* **2007**, *111*, 15440–15445.

(55) Van Der Stam, W.; Grimaldi, G.; Geuchies, J. J.; Gudjonsdottir, S.; Van Uffelen, P. T.; Van Overeem, M.; Brynjarsson, B.; Kirkwood, N.; Houtepen, A. J. Electrochemical Modulation of the Photophysics of Surface-Localized Trap States in Core/Shell/(Shell) Quantum Dot Films. *Chemistry of Materials* **2019**, *31*, 8484–8493.

(56) Albery, W. J.; Bartlett, P. N.; Porter, J. D. The Electrochemistry of Colloidal Semiconductor Particles: Theory. *Journal of The Electrochemical Society* **1984**, *131*, 2892–2896.

(57) Albery, W. J.; Bartlett, P. N.; Porter, J. D. The Electrochemistry of Colloidal Semiconductor Particles: Experiments on CdS and TiO2. *Journal of The Electrochemical Society* **1984**, *131*, 2896–2900.

(58) Carroll, G. M.; Tsui, E. Y.; Brozek, C. K.; Gamelin, D. R. Spectroelectrochemical measurement of surface electrostatic contributions to colloidal CdSe nanocrystal redox potentials. *Chemistry of Materials* **2016**, *28*, 7912–7918.

Acknowledgement

The authors thank the ARC for support through CE170100026. A.A thanks the University of Melbourne for a Melbourne Research Scholarship.

Supporting Information Available

Geometry of working electrode

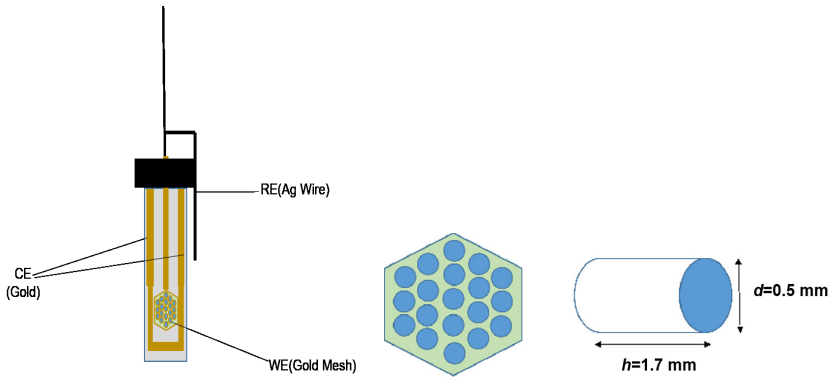

Figure S 1: (a) Diagram of the spectroelectrochemical cell. (b) Enlarged view of the working electrode which consists of 19 cylindrical holes. The interior of the cylinder is coated with either gold or platinum. The length and diameter of each cylinder is 1.7 mm and 0.5 mm respectively.

Calibration of the electrode

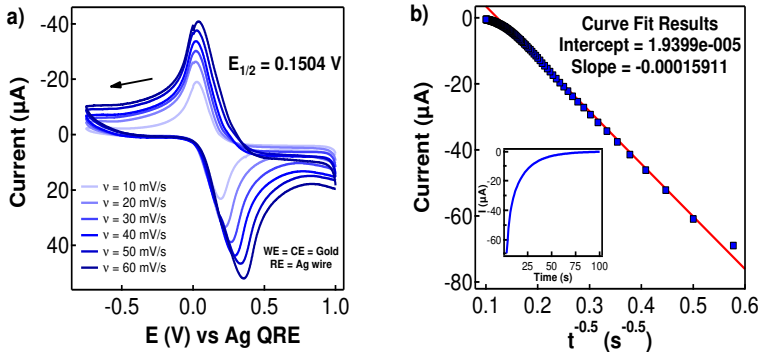

Figure S 2: (a) Cyclic voltammetry of ferrocene in 0.1 M $TBAPF_6$ in THF at different scan rate (ν) (b) Cottrell plot of current measured for (blue square) of 2 mM ferricyanide in 1 M KNO_3. The inset shows the corresponding chronoamperometric curve.

Determination of effective electrochemical Area: Chronoamperometry was used to determine the effective area of the SEC electrodes. In the diffusion-limited regime, the measured current (i_d) can be related to the time (t) and the number of electrons injected

(n) through the Cottrell equation:

$$i_d = nFAC\sqrt{\frac{D}{\pi t}}$$

where F is the Faraday constant, A is the effective electrochemical surface area, D is the diffusion coefficient and C is the initial concentration. This holds true only for a planar electrode and is widely used in electrochemistry to determine the number of electrons involved in a redox reaction, the diffusion coefficient of an analyte and the area of the workkking electrode. Due to the cylindrical geometry of the working electrode, cylindrical diffusion takes place at the working electrode. Solving for the transient current time relationship in the cylindrical diffusion case adds a constant component and an augmentative component (whose magnitude increases with time) to the usual Cottrell equation.

$$i_d = nFAC\left(\sqrt{\frac{D}{\pi t}} + \frac{D}{2r} - \sqrt{\frac{D^3 t}{16\pi r^4}} + \frac{D^2 t}{8r^3} + ...\right)$$

If the potential step experiments are conducted on a shorter time scale, the augmentative component fades away and the equation reduces to the usual Cottrell equation with an additional constant term.

$$i_d = nFAC\left(\sqrt{\frac{D}{\pi t}} + \frac{D}{2r}\right)$$

Hence from the slope of the i_d vs $t^{-0.5}$ plot, the number of electrons injected can be determined. The validity of this expression was checked using potential step measurements with ferricyanide solutions and this yielded an excellent fit to the Cottrell equation (See Figure S2b) from which we obtained 0.48 cm^2 as the effective area of the SEC honeycomb electrodes, which is close to the geometric area of 0.50 cm^2. The current measured during a potential step can be integrated to yield the charge transferred to the QDs. The charge Q measured is proportional to the $\sqrt{t}$ and exhibits a linear relationship in a Q vs $\sqrt{t}$ plot.

This is known as the Anson equation and connects Q measured and the $\sqrt{t}$ as follows:

$$Q = 2nFAC\sqrt{\frac{Dt}{\pi}} + Q_{ads} + Q_c$$

where Q_{ads} and Q_c are the charge due to any adsorbed electroactive species and the double layer charge respectively.

Absorption and emission spectra of QD samples

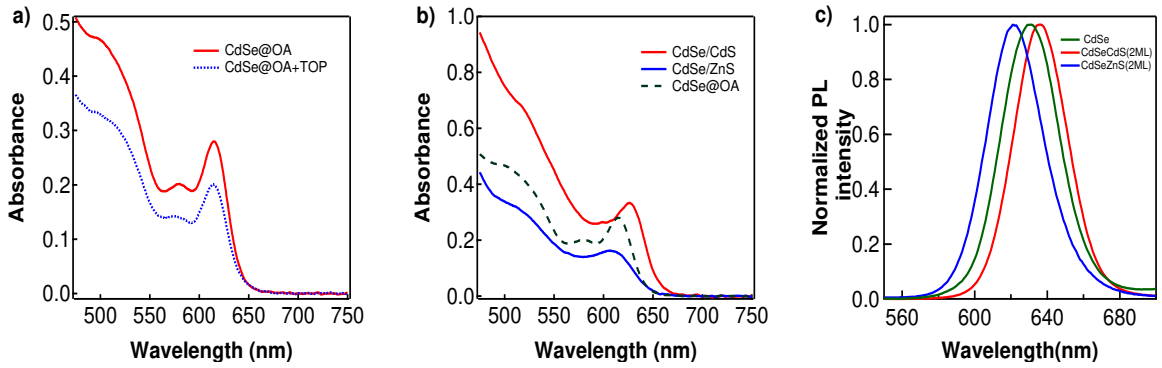

Figure S 3: (a) Absorption spectra of CdSe capped with oleic acid (d=5nm) and after exchange with TOP. (b) Absorption spectra of CdSe QD (Dark green dashed line), CdSe/CdS (Red line) and CdSe/ZnS (Blue line) and (c) Emission spectra of CdSe, CdSe/CdS, CdSe/ZnS.

Electrochemical characterization of CdSe QDs

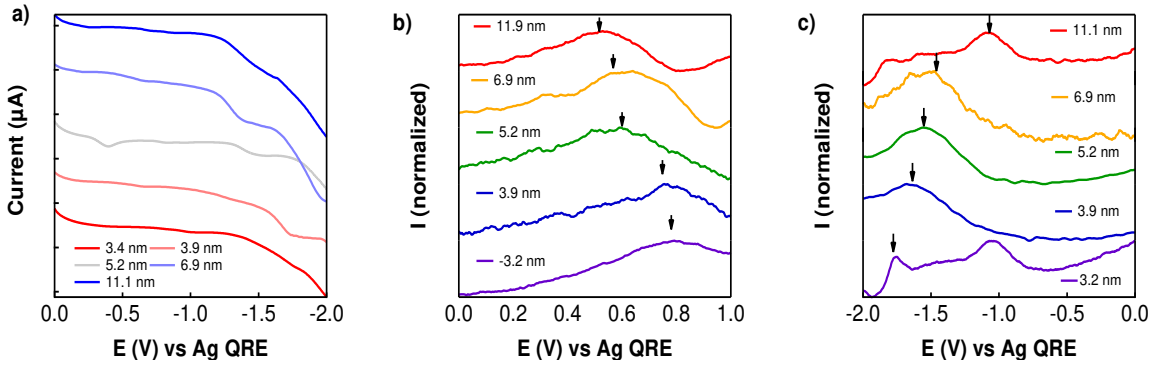

Figure S 4: (a) Linear sweep voltammetry ($\nu = 10$ mV/s), and Differential pulse voltammetry of CdSe QDs of different size in 0.1 M $TBAPF_6$ in dry and deaerated THF during (b) anodic and (c) cathodic scan respectively. The OD of all QDs at excitonic peak was 0.15. Current measured during the DPV of all QDs are normalised with respect to their corresponding peak maximum. The arrows indicate the peak positions of each scan. DPV parameters: modulation time = 50 ms; internal time = 500 ms; step potential = 5 mV;modulation amplitude = 25 mV; scan rate = 10 mV/s.

Spectroelectrochemical determination of conduction band edge in CdSe

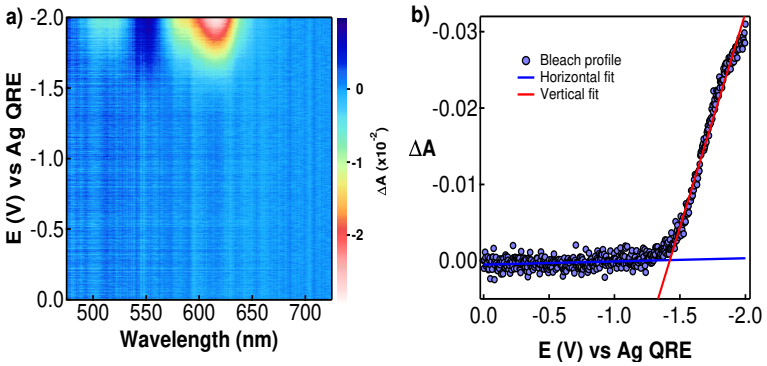

Figure S 5: (a) 2D difference spectra of QD (d = 5.24 nm) obtained during the linear sweep voltammetry from 0 V to -2 V at a scan rate of 10 mV/s. The spectrum starts to bleach at potentials more negative than -1.5 V. (b) Fit of ΔA vs E(V) for the estimation of CB potential. The blue and red line represents the linear fit corresponding to the baseline and bleach respectively. The intersection point of the two fit is taken as the CB potential.

QD stability during charge injection

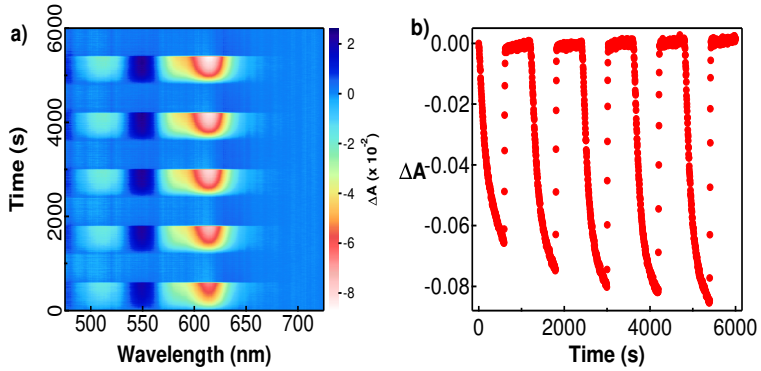

Figure S 6: (a) 2D Difference absorption spectra of CdSe QD (d = 5.24 nm) and (b) Corresponding change in first exciton absorption peak ($1S_{3/2h}$-$1S_e$ transition) during the potential cycling between -1.5V and 0V. Each step was applied for 600 s.

Electrons injected during potential step

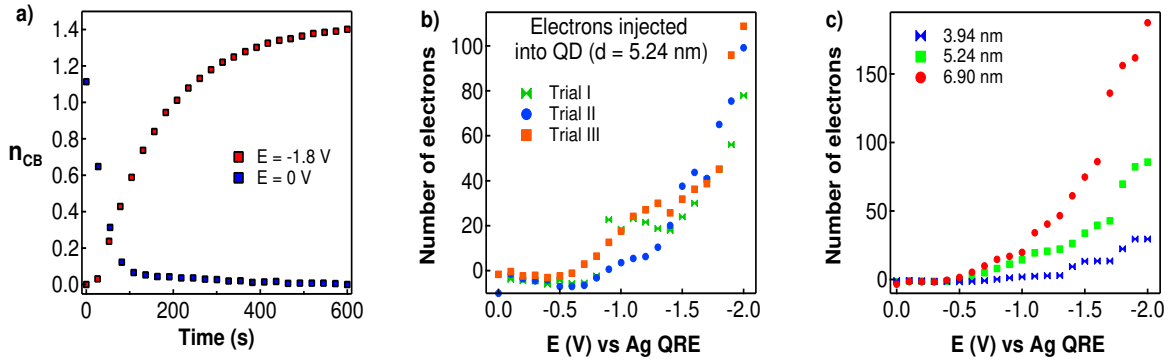

Figure S 7: (a) Electrons (n_{CB}) injected during the potential step at -1.8 V (Red square) and decayed at 0 V (Blue square) calculated from the absorption bleach ($\Delta A = A_t - A_0$) using the equation: $n_{CB} = -2\frac{\Delta A}{A_0}$, where A_t and A_0 are the absorbance corresponding to the $1S_{3/2h}$-$1S_e$ transition at time t and 0 seconds respectively. (b) Electrons injected into QD(d = 5.24 nm) during the potential step calculated using Cottrell equation for three different trials. Trials II and III have the same absorbance of 0.15 at the exciton peak while trial I has an absorbance of 0.125 at the exciton peak. (c) Electrons injected into QDs into three different sized QD during the potential step calculated using Anson equation.

PL intensity during linear potential sweep

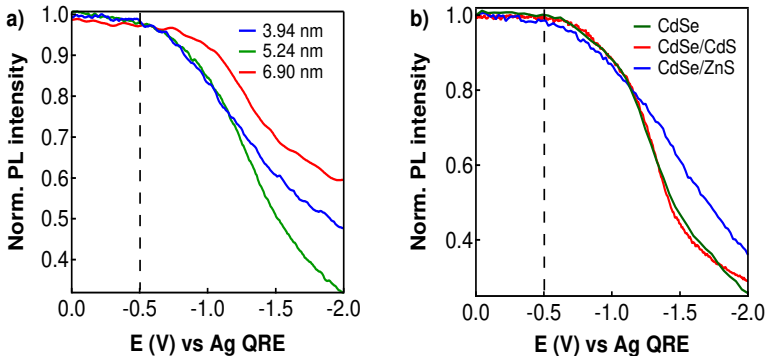

Figure S 8: Change in photoluminescence intensity during a potential sweep from 0 V to -2 V ($\nu = 10$ mV/s) (a) for CdSe QDs of three different sizes and (b) for CdSe QDs, CdSe/CdS QDs and CdSe/ZnS QDs.

Diffusion controlled bleach and recovery of exciton peak

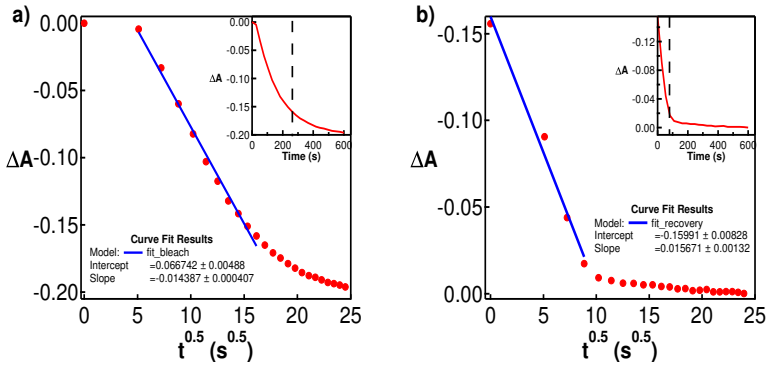

Figure S 9: (a) Exciton bleach profile during a potential step of -1.8 V vs $t^{0.5}$ (Red sphere) and corresponding linear fit (Blue trace). (b) Recovery profile during the potential step of 0 V vs $t^{0.5}$(Red sphere) and corresponding linear fit (Blue trace). The inset in graphs shows the bleach/ recovery profile vs time. Linear dependence of two profiles to square root of time at shorter time scales shows that both are controlled by diffusion. The dotted line in inset shows the time at which the effects of diffusion is reduced.

Potential dependent recovery of exciton absorption

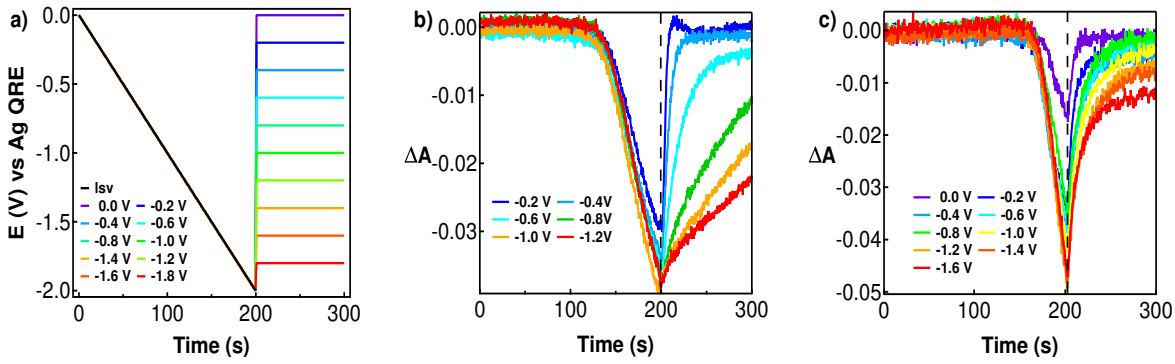

Figure S 10: (a) The potential sweep-step applied for studying the potential dependent recovery of injected electrons.The sweep was at a scan rate of 10 mV/s and the potential step was applied for 100 s. Change in exciton absorption peak of CdSe QD of size (b) 5.24 nm and (c) 3.94 nm in response to potential sweep step. The traces were labelled according to the potential step applied following the sweep. The black dotted line indicate the point at which the potential sweep switch to step. The duration of potential step was 100 s.

2D difference spectra of QD in response to potential step

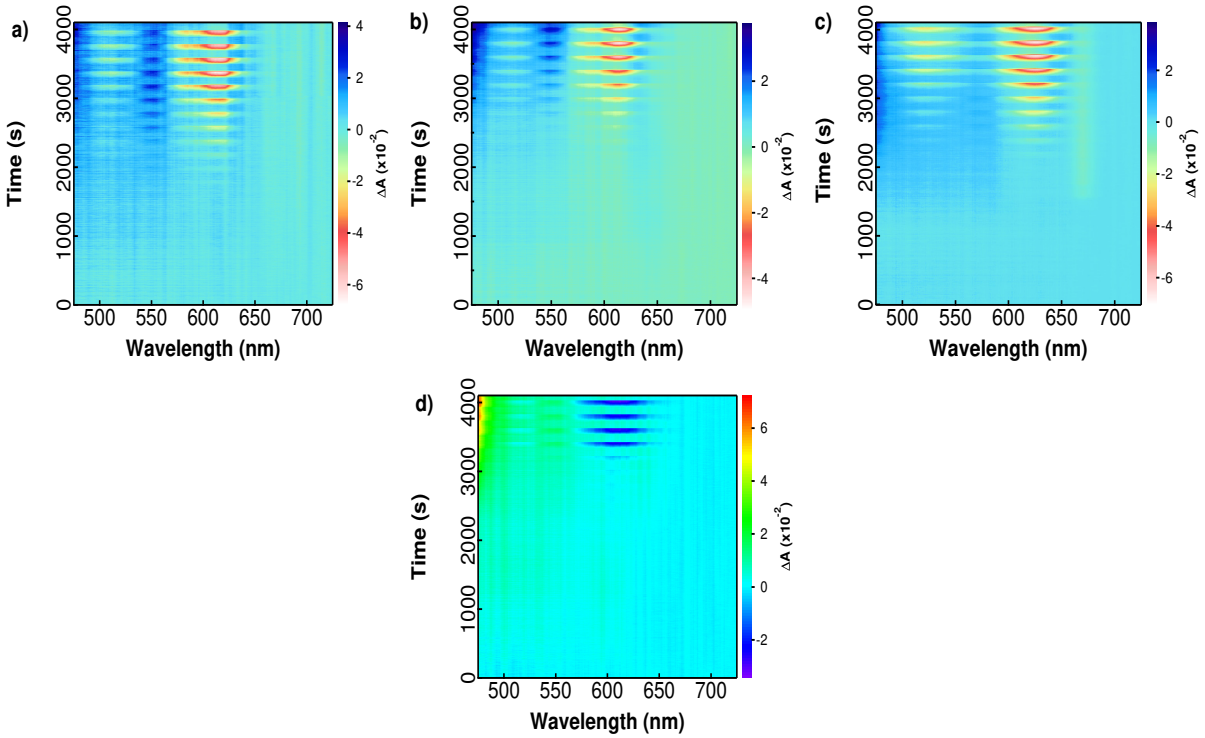

Figure S 11: 2D difference spectra of (a) CdSe capped with Cd-oleate, (b) after ligand exchange with TOP, (c) CdSe/CdS and (d) CdSe/ZnS.

Graphical TOC Entry